




REGULAR ARTICLE

Equivalent Circuit Model to Reach Complicated Surface Photovoltage Transient Shapes in ZnO Thin Films

A. Nadtochiy^{1,*} , A. Podolian¹, O. Korotchenkov¹, O. Oberemok², O. Kosulya², B. Romanyuk²

¹ Faculty of Physics, Taras Shevchenko National University of Kyiv, 01601 Kyiv, Ukraine

² V. Lashkarev Institute of Semiconductor Physics NAS of Ukraine, 03028 Kyiv, Ukraine

(Received 22 January 2024; revised manuscript received 18 April 2024; published online 29 April 2024)

The dynamics of photoexcited carriers in magnetron sputtered ZnO films is characterized employing time-domain impedance analysis, which is based on the measurements of the surface photovoltage (SPV) transients. The studies focus on observing the damage after the implantation of Nd⁺ ions in ZnO layers and a subsequent anneal. We observed the positive and negative components of the measured SPV transient and develop equivalent circuits of the structure involving multiple series of parallel resistance (R), capacitance (C), and inductance (L) elements, and derive a simple fitting procedure which allows to reproduce accurately the measured SPV transient. The relationship between these RCL elements and a rough physical picture of the charge transport phenomena in the interface regions of the structure is envisaged. This approach is conceptually useful for characterizing interfaces in semiconductor structures and devices.

Keywords: Surface Photovoltage, Zinc Oxide, Equivalent Circuits.

DOI: [10.21272/jnep.16\(2\).02023](https://doi.org/10.21272/jnep.16(2).02023)

PACS numbers: 72.20.Jv, 73.50.Pz

1. INTRODUCTION

There has been a significant advance in our understanding of interfacial electronic properties and band bending in semiconductors at the substrate/layer interface. To describe carrier dynamics in the space charge interface region surface photovoltage (SPV) decays can be used. As previously reported, ZnO surfaces may show the short-time dynamic behavior ranging from a few hundred μ s to about 1 ms, perhaps due to persistent photoconductivity [1]. The full description of this effect in ZnO is complicated, and a large number of contributions have been commonly considered to be essential to the understanding of the persistence of photoconductivity after switching off the exciting light. Notable among these are the hole capture from the surface depletion layer by chemisorbed O²⁻, metastable doubly or singly charged oxygen vacancies, loss of lattice oxygen, H₂ molecules trapped at oxygen vacancy sites (for details see Ref. [1] and references therein).

It is clear, therefore, that all the above mentioned consequential effects must be taken into account in the equivalent circuit. One should then bear in mind that it is somewhat difficult to derive physically meaningful conclusions based on cumulative behaviors of model circuits. Nevertheless, the frequency (ω) – and time (t) – domain impedance measurements are widely used for the parametrization of equivalent circuit models [2, 3].

Analysis of the frequency-dependent capacitance and conductance uses an equivalent circuit, which can take into account effects of interface states. This approach is focused on the simplest equivalent electrical circuit where

resistance (R), capacitance (C), and inductance (L) elements reproduce the impedance of the measured structure. Additional elements, e.g. the constant phase element (CPE), can be supplemented to address a nonideal capacitor behavior. The equivalent circuits with CPEs were also used to tackle the problem of surface roughness, leakage capacitance and nonuniform charge distribution in semiconductor-insulator systems that result in the nonideal capacitor behavior [4-6].

Here, we derive a simple time-domain model for fitting the SPV transient curves employing multiple series of parallel RCL elements. The analysis is applied to the SPV data of magnetron sputtered ZnO films, as-grown, implanted with Nd⁺ ions, and subsequently annealed. Varying the RCL parameters yields an excellent agreement between the fitting curves and the measured data.

2. EXPERIMENTAL DETAILS

Experimental SPV decay curves were taken in ZnO films with a thickness of about 70 nm. The films were deposited onto p -Si (100) substrates at room temperature by the RF reactive magnetron sputtering using a ceramic aluminum-doped zinc oxide (AZO) (98 wt% ZnO + 2 wt% Al₂O₃) target with a purity of 99.99 %. Details of the growth procedure were given elsewhere [7]. Here, we compare the SPV decay properties of the resulting ZnO films before (undoped ZnO) and after (ZnO:Nd) room temperature implantation of Nd⁺ ions with the energy of 75 keV and dose rate of 5 μ C/cm². The results presented below were obtained in the samples furnace annealed at 650°C in the argon

* Correspondence e-mail: nadtku@univ.kiev.ua



flow during 30 min.

The bandgap (E_g) is 3.2–3.3 eV in ZnO [8] and 1.12 eV in Si [9]. This means apparently that exciting light with the wavelength of about 375 nm corresponds to E_g in ZnO. As a result, irradiation of such a ZnO/Si structure by visible light excites free carriers predominantly in the Si substrate. For the light with a wavelength of less than 375 nm, the SPV signal will come from both the ZnO film and Si substrate. Evidently, irrespective of the selected wavelength the excited carriers can migrate from Si to ZnO and in the opposite direction. In our SPV measurements, a 275 nm (or 4.51 eV) LED light from ProLight Opto PB2D-UCLA-TC was used as excitation source. The absorption coefficient in ZnO thin film at the wavelength of 275 nm is of order of $1.5 \times 10^5 \text{ cm}^{-1}$ [10], which corresponds to the penetration depth of about 70 nm. With these assumptions, the contribution of the carriers excited in Si was minimized. The SPV data given below were measured in the capacitance arrangement, as described in detail elsewhere [11].

3. RESULTS AND DISCUSSION

Fig. 1 shows typical SPV transient curves observed in ZnO (curve 1) and ZnO:Nd (2) films. The essence of the effects can be captured by decomposing the decaying part of the SPV data into transients with positive and negative values of the SPV signal magnitude. The sum of them may produce the shape given by curve 1 in Fig. 1. Essentially, the negative signal is largely suppressed in curve 2. This observation implies that there is an alternative source of the spatially separated electrons and holes, which is most likely related to the band bending features of the structure modified by the implantation of Nd⁺ ions.

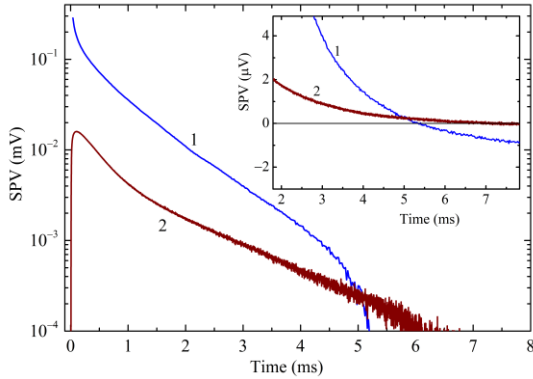


Fig. 1 – Measured SPV transients in ZnO (1) and ZnO:Nd (2) films annealed at 650 °C. The duration of the exciting light pulse is 12 μs . Inset illustrates a portion of the curves near the crossover point displayed on a linear SPV scale

Irrespective of the basic physical picture describing the data of Fig. 1, here we aim to refine the treatment of complicated SPV decay curves with the contributions that have opposite sign. We employ equivalent circuit modeling which uses the time-domain impedance analysis.

3.1 Modeling SPV Decays

For an account of experiments, we start with fitting curve 2 in Fig. 1 to a network of RC circuits. Then, the

model will be applied to the SPV transient with the sign inversion (curve 1 in Fig. 1) by introducing RCL units.

Thus we can consider the basic schematic diagram of the SPV measurement shown in Fig. 2. The SPV decay is formed by the Z_1 - Z_3 elements which are combined with simple RCL components. The other circuit elements, R_1 - R_3 , C_1 and C_2 , belong to the SPV signal amplification scheme, which was considered elsewhere [12].

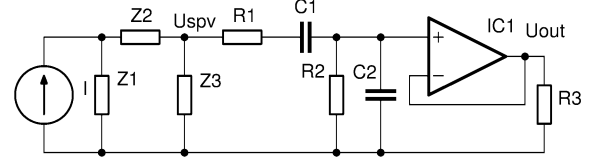


Fig. 2 – Equivalent circuit for SPV measurement arrangement. I – photo-generated current, U_{SPV} is the generated SPV signal

Despite equivalent schemes describing SPVs have been known for a long time, the schemes found in the literature are not directly applicable to the modeling of transient processes during the SPV relaxation. Thus, in Ref. [13] an equivalent circuit was given to describe the SPV which consists of a capacitor and a resistor connected in parallel, as shown in Fig. 3(a). The capacitor in such a scheme is associated with charge accumulation processes while the resistor accounts for recombination processes. This simple scheme describes only a simple single-exponential decay curve (like line 2 in Fig. 5) and is not suitable for analysis of our experimental data. Therefore, for an adequate description of the decay curves, we must add other elements to the equivalent circuit that are necessary to explain the shape of the SPV decays. For example, in order to explain the prolonged SPV decays seen in Fig. 1 (curve 2), additional elements C_1 and R_1 in Fig. 3(b) were added to the equivalent circuit shown in Fig. 3(a).

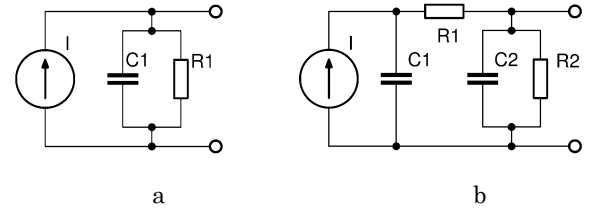


Fig. 3 – Equivalent circuit for ac surface photovoltage [13] (a), equivalent circuit providing a dashed line fit (Fig. 6) for the experimental SPV transient curve (b)

For the purposes of transient analysis, we employ a two-step procedure. First, the voltage U_{SPV} vs applied current I is calculated. Second, the values of I , C_1 , R_1 , C_2 and R_2 are adjusted to minimize the difference to the measured SPV transient. In this analysis, theory of electrical circuits [14] is applied to obtain a useful form for the SPV transient.

Using the Kirchhoff's laws we first equate $I_R = U_R/R$, $I_C = C dU_C/dt$ and then arrive at the system of ordinary differential equations

$$\begin{bmatrix} \frac{du_{C1}}{dt} \\ \frac{du_{C2}}{dt} \end{bmatrix} = \begin{bmatrix} -\frac{1}{C_1 R_1} & \frac{1}{C_1 R_1} \\ \frac{1}{C_2 R_1} & -\frac{1}{C_2 R_1 R_2} \end{bmatrix} \begin{bmatrix} u_{C1} \\ u_{C2} \end{bmatrix} + \begin{bmatrix} \frac{I(t)}{C_1} \\ 0 \end{bmatrix}. \quad (1)$$

Here, U_{C1} and U_{C2} are the voltages on the capacitors C_1 and C_2 while the current I is calculated as a function of time $i(t)$ multiplied by the light pulse amplitude, $I = AIP i(t)$.

The above system is solved using the Backward Euler method [14], which results in $U_{SPV} = U_{C2}$. Then, to adjust I , C_1 , R_1 , C_2 and R_2 , the BOBYQA algorithm for bound constrained optimization without derivatives from NLOpt program library [15] is used, which allows us to compute the time-dependent U_{SPV} .

The best fit to the measured data shown by the dashed line in Fig. 5 is obtained with $C_1 = 2.1$ nF, $R_1 = 11$ k Ω , $C_2 = 1.12$ μ F, and $R_2 = 564$ Ω . As seen in Fig. 5, the equivalent circuit of Fig. 3(a) does not provide a suitable fit (dashed line) for the measured decaying part of the SPV transient curve (circles). Meanwhile, there is a convincing agreement between fitted and experimental results at the rising part of the SPV transient.

Evidently, while the light is switched on at $t = 0$, light induced charge carriers recombine with the rate averaged over the available radiative and non-radiative pathways. They are partly immobilized due to trap capture. The carriers remain captured until they are thermally released back into the electron and hole energy bands or recombine and disappear. As a result, having the light switched off at some preceding time ($t = 12$ μ s in Fig. 5), we see a rise in the SPV signal even after the termination of the light pulse (up to about 100 μ s in Fig. 5).

With these issues, if C_1 and R_1 are removed from the circuit of Fig. 3(b), the C_2 and R_2 elements describe a single exponential decay. The C_1 and R_1 elements form a delay circuit, which in turn gives a contribution to the rising SPV. Electrical energy would accumulate in C_1 under pulse excitation, and at the pulse termination flows into the C_2 and R_2 elements through R_1 . As a result, the rising behavior is interpreted in terms of the equivalent circuit shown in Fig. 3(b).

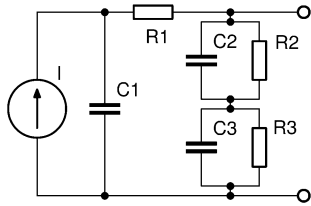


Fig. 4 – Equivalent circuit providing a continuous line fit (Fig. 5) for the experimental SPV transient curve

The decay behavior of interest obtains only if the transient process is represented by the modified equivalent scheme shown in Fig. 4. In the analysis described above, the system of differential equations can be rewritten as

$$\begin{bmatrix} \frac{du_{C1}}{dt} \\ \frac{du_{C2}}{dt} \\ \frac{du_{C3}}{dt} \end{bmatrix} = \begin{bmatrix} -\frac{1}{C_1 R_1} & \frac{1}{C_1 R_1} & \frac{1}{C_1 R_1} \\ \frac{1}{C_2 R_1} & -\frac{1}{C_2 R_1 R_2} & -\frac{1}{C_2 R_1} \\ \frac{1}{C_3 R_1} & -\frac{1}{C_3 R_1} & -\frac{1}{C_3 R_1 R_3} \end{bmatrix} \begin{bmatrix} u_{C1} \\ u_{C2} \\ u_{C3} \end{bmatrix} + \begin{bmatrix} I(t) \\ C_1 \\ 0 \end{bmatrix} \quad (2)$$

in the usual notations. By carefully optimizing I , C_1 , R_1 , C_2 , R_2 , C_3 and R_3 we have $U_{SPV} = U_{C2} + U_{C3}$, which

is plotted by continuous line in Fig. 5. As seen, this equivalent scheme strongly improves the agreement with experiment (circles in Fig. 5).

We suggest, therefore, that the rising and decaying behavior is indicative of recombination and trapping processes occurring in the films on a relevant range of time scales, an assertion for which there is some above evidence. C_1 and R_1 contribute to the rise part of the transient voltage, as already discussed. Efficient spatial electron-hole separation is corroborated by R_1 , which acts as a charge-transfer state. Smaller values of R_1 enable charge carriers to accelerate to higher velocities in a less pronounced scattering thus providing a more efficient way of separating e^- and h^+ .

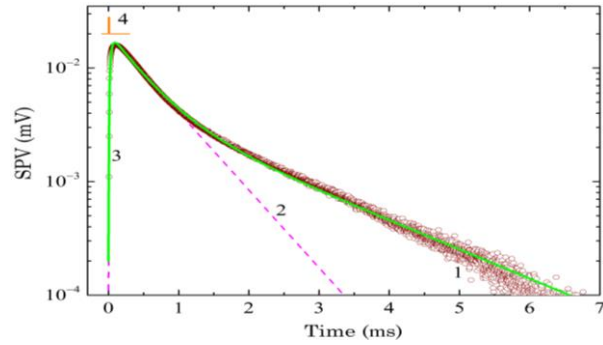


Fig. 5 – SPV transient in ZnO:Nd film (circles, curve 2 in Fig. 1) fit with the equivalent circuits of Fig. 3(b) (dashed line 2) and Fig. 4 (continuous line 3). The 12- μ s excitation-pulse position on the time scale is marked (line 4)

3.2 Equivalent RCL electrical circuit approach for transient SPV analysis

Our overall approach is that the idea of an equivalent RC circuit model contains the essence of the charge carrier decay dynamics and gives a quantitative footing for modeling the SPV transient without the sign inversion. Complementing our simulations by the inductance elements gives us a reasonable account of the sign inversion in the SPV decay. To capture this inductance property, it is more convenient to refer to the circuit shown in Fig. 6.

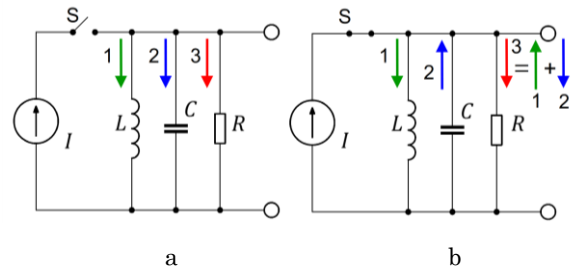


Fig. 6 – Equivalent electric scheme explaining the SPV sign inversion. Switch S is used to drive the circuit with the feeding photocurrent I during the light is switched on (a) and off (b). Arrows indicate current directions in inductance L (1), capacitance C (2), and resistance R (3)

When the switch S is closed in Fig. 6(a), the current source I starts charging the capacitance C , simultaneously increasing the voltage across the resistance R and the current through the inductance L . Appropriate current directions are marked by arrows 1–3 in Fig. 6(a).

Opening the switch in Fig. 6(b) gives rise to reverse current marked by arrow 2, which discharges C through R . It is also clear that the current through L does not change its sign (arrow 1) showing a decreased contribution to the current through R . The sum of the currents marked by arrows 1 and 2 forms a voltage drops across the resistance R , and the voltage polarity is reversed when the two currents are equal and opposite.

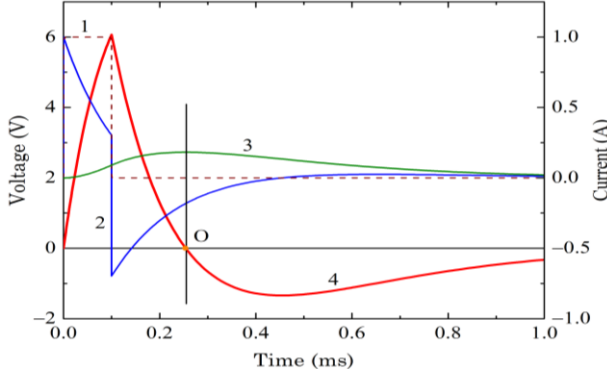


Fig. 7 – Transient processes in the scheme of **Fig. 6** at $L = 4$ mH, $C = 10$ μ F, and $R = 10$ Ω . 1 – single square current pulse with a width of 0.1 ms, 2 – current through capacitance C , 3 – current through inductance L , 4 – voltage drop across the resistance R . O – crossover point for the voltage across R

Using the Kirchhoff's laws, we can write an equation of the transient process in the scheme of Fig. 6(a), according to which the sum through all elements of the circuit (connected in parallel) is equal to the current of the source I [16]:

$$I_C(t) + I_R(t) + I_L(t) = I(t), \quad t \geq 0, \quad (3)$$

where I_C , I_R , I_L – currents through capacitance C , resistance R and inductance L , according. Taking the current through the inductance as an independent value and using the element equations of the resistance $U_R = I_R R$, capacitance $I_C = C dU_C/dt$, and inductance $U_L = L dI_L/dt$ we write (3) in the form

$$\frac{d^2 I_L(t)}{dt^2} + \frac{1}{RC} \frac{dI_L(t)}{dt} + I_L(t) = \frac{1}{LC} I(t), \quad t \geq 0, \quad (4)$$

We seek a particular solution to the associated homogeneous differential equation in the form

$$I_L(t) = A_1 e^{-s_1 t} + A_2 e^{-s_2 t}, \quad (5)$$

where A_1 and A_2 are the constants, $s_{1,2} = \left(\xi \pm \sqrt{\xi^2 - 1} \right) \omega_0$ are the natural frequencies, $\omega_0 = 1/\sqrt{LC}$ is the undamped natural frequency, $\xi = R_{cr}/R$ is the damping factor and $R_{cr} = 1/2 \sqrt{L/C}$ is the critical resistance.

For the aperiodic type of behavior of current, corresponding to $\xi \gg 1$, a simple approximate is

$$s_1 \approx 2\xi \cdot \omega_0 = \frac{1}{RC} = \frac{1}{\tau_1}, \quad (6)$$

$$s_2 \approx \frac{1}{2\xi} \cdot \omega_0 = \frac{R}{L} = \frac{1}{\tau_2}, \quad (7)$$

Thus a bi-exponential decay with the time constants $\tau_1 = RC$ and $\tau_2 = L/R$ is observed. If τ_1 is sufficiently large compared with τ_2 , the reverse of U_R happens at the time the balance of I_L and I_C is reached. This is illustrated by curve 4 in Fig. 7, which models the dynamical quantities of the circuit in Fig. 6.

The essence of the problem is readily seen in Fig. 7. However, experimentally we know that the charge dynamics would tend to maintain a multi-exponential decay. Therefore, more generally, the impedance network can consist of multiple series-connected parallel RCL units. However, circuits with RCL s may require a fewer number of units for modeling SPV decays, if some small number of recombination and capture pathways are assumed. Fig. 8 shows an 10-section RCL equivalent circuit of the model.

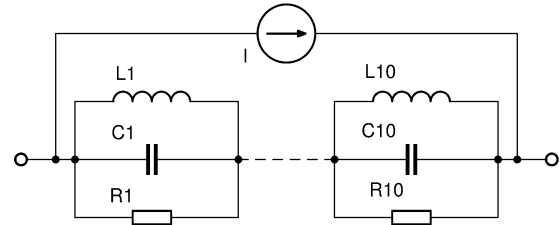


Fig. 8 – Ten-section RCL equivalent circuit to represent the SPV decay

The next equivalent circuit to be considered asserts that the fitting form for transients with the contributions that have opposite sign can be constructed with RCL units (Fig. 8). The SPV decay curve 1 in Fig. 1 can then be fitted with the circuit shown in Fig. 8 that have n RCL units. We therefore arrive at the following expression

$$\begin{bmatrix} \frac{du_{C1}}{dt} \\ \frac{du_{Cn}}{dt} \\ \frac{di_{L1}}{dt} \\ \frac{di_{Ln}}{dt} \end{bmatrix} = \begin{bmatrix} -\frac{1}{C_1 R_1} & 0 & -\frac{1}{C_1} & 0 \\ \cdot & \cdot & \cdot & \cdot \\ 0 & -\frac{1}{C_n R_n} & 0 & -\frac{1}{C_n} \\ \frac{1}{L_1} & 0 & 0 & 0 \\ \cdot & \cdot & \cdot & \cdot \\ 0 & \frac{1}{L_n} & 0 & 0 \end{bmatrix} \begin{bmatrix} u_{C1} \\ u_{Cn} \\ i_{L1} \\ i_{Ln} \end{bmatrix} + \begin{bmatrix} I(t) \\ \frac{I(t)}{C_1} \\ \frac{I(t)}{C_n} \\ 0 \\ \cdot \\ 0 \end{bmatrix}, \quad (8)$$

where the subscript n is related to the n -th RCL unit. The fitting result for $n = 10$ is depicted in Fig. 9. The model provides an excellent fit to decay data.

Contrary to the experimentally obtained transient behavior, the development of equivalent circuit models is somewhat contentious. The challenge is how to relate the transient composed of instantaneous decay lifetimes to particular recombination and capture pathways. These pathways do not necessarily directly contribute to any exponential deconvolution of the transient curve. A popular notion is that the relaxation of carrier-confined large ensembles in inhomogeneous structures exhibits a multiexponential or stretched-exponential form [18]. With these assumptions, the decay can initially be related to direct carrier recombina-

nation and capture processes, until various distributions of trapping centers are filled. Further, the decay curve elongation is attributed to carrier capture and trapping lifetimes because they exceed those of carrier recombination. It is quite obvious that both of the multi-exponential or stretched-exponential forms usually provide suitable fits for the experimental decay curves by increasing the number of summands.

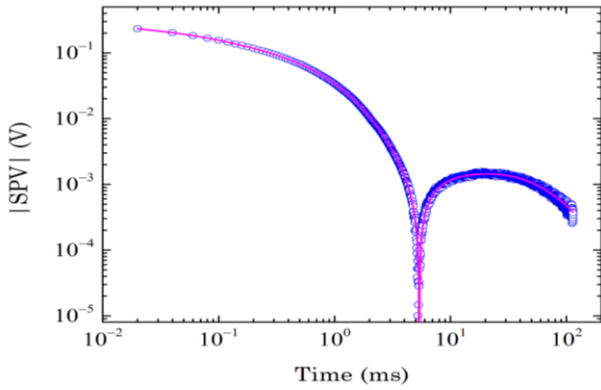


Fig. 9 – SPV decay in ZnO:Nd film (circles, curve 1 in **Fig. 1**) fit with the ten-section RCL equivalent circuit of **Fig. 8** (line). The negative portion of the decay at times greater than \square 5 ms is reversed when plotted on a log scale

However, the usage of RC components of the equivalent circuit is often not rigorously valid as the dynamic charge transfer processes can be spatially distributed producing a broad spectrum of time constants [19]. This can be cast into a constant phase element language, which substitutes capacitors in the equivalent circuit models and reduces a number of relevant parameters. The CPE is defined in the frequency domain with the impedance of $Z_{CPE} = 1 / C_0(j\omega)^\gamma$, where j is the imaginary unit, $\gamma \in [0,1]$ is the dispersion coefficient, and C_0 is the frequency independent capacitance related to the double junction capacitance in our case.

Significantly, many of the CPE implementations are formulated in the frequency domain, whilst the direct time-domain modeling approach still remains somewhat controversial. Nevertheless, it is illustrative to consider the multiple RC circuit, high-order integer transfer function, and the Grünwald–Letnikov fractional derivative approximations [19, 20], which give us a coherent account of the available time-domain implementations. Based on our encouraging fitting results, it is foreseeable that introducing inductance L into the equivalent circuit in fact offers an effective means of studying SPV decays.

The naive expectation for a consistent physical picture of L , which is based on the elongated decay, predicts that the charge carriers of one sign are captured into interface trapping levels, whereas carriers of the opposite sign drift outside the space charge region in the processes 2' and 5 (Fig. 10) for electrons or 3' and 6 for holes. The following trap-release of carriers will eventually explain the elongation of SPV dynamics decay being controlled by the subsequent excess carrier recombination. The occurrence of random delays that impede the recombination of separated e^- and h^+ will therefore drive the electrical current carried by the released charges. It makes good sense to consider this to be the current

through inductance in the circuit of Figs. 6 and 8 that oppose a change in the I_L flowing through L .

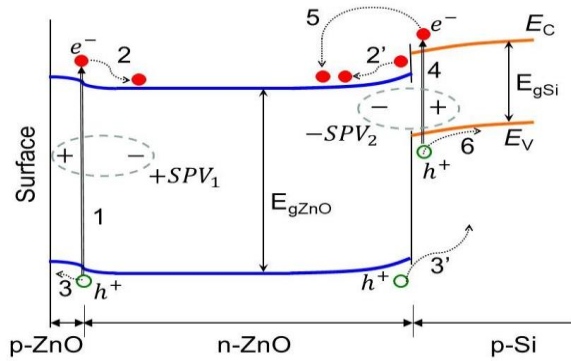


Fig. 10 – Schematic energy band diagram of our ZnO/p-Si structure. Conduction and valence band alignments are given for the ZnO/Si interface [21]. The homo- and heterojunction contributions to SPV ($+SPV_1$ and $-SPV_2$, respectively) are illustrated

Finally, it is illustrative to consider the frequency distribution of random delay times $\tau_{i_i} = R_i C_i$ in the i -th pathway, which impedes the recombination of excess carriers and prolong the observed SPV decays. As a result, we have a broad distribution of τ_{i_i} in the ZnO film shown in Fig. 11, implying a number of exponential decompositions of the decay curve. For comparison, the RCL fitting result for the ZnO:Nd film is also shown in Fig. 11. Evidently, the SPV decay curve in ZnO:Nd can then be represented as a convolution of two time variables, as is indeed the case in Fig. 5.

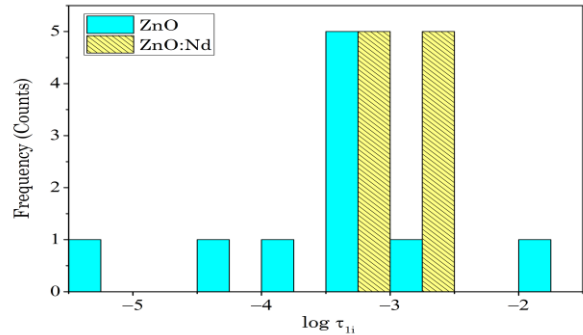


Fig. 11 – Probability of occurrences of particular values of random delay times τ_{i_i} in ZnO and ZnO:Nd films, which are obtained by fitting the SPV decays in **Fig. 1** (curves 1 and 2) to the ten-section RCL equivalent circuit ($i = 1 \dots 10$) of **Fig. 8**.

4. CONCLUSIONS

In summary, complicated SPV transients with the contributions which are opposite in sign can be described by the equivalent RCL circuit model. The time-domain fitting technique, reproducing the measured SPV transient, is derived. Our overall finding is that multiple units, which consist of an ohmic resistor in parallel with a capacitor, model the SPV transient without the sign inversion. For a suitable representation of the sign inversion in the SPV decay, we propose an inductance as the equivalent circuit element, which is combined in parallel with the RC unit. The model is applied to investigate

ZnO and ZnO:Nd thin films and the implantation-induced damage in the films. The film quality, especially near the film/substrate interface, can be deduced by analyzing the SPV decay. A similar approach may be advan-

tageous for modeling electrochemical charge transfer processes that occur at different rates including, for example, the movement of charge carriers through the electrolyte in batteries and fuel cells.

REFERENCES

1. B.F. Spencer, D.M. Graham, S.J.O. Hardman, E.A. Seddon, M.J. Cliffe, K.L. Syres, A.G. Thomas, S.K. Stubbs, F. Sirotti, M.G. Silly, P.F. Kirkham, A.R. Kumarasinghe, G.J. Hirst, A.J. Moss, S.F. Hill, D.A. Shaw, S. Chattopadhyay, W.R. Flavell, *Phys. Rev. B* **88**, 195301 (2013).
2. M. Gabás, E. Ochoa-Martínez, E. Navarrete-Astorga, A.R. Landa-Cánovas, P. Herrero, F. Agulló-Rueda, S. Palanco, J.J. Martínez-Serrano, J.R. Ramos-Barrado, *Appl. Surf. Sci.* **419**, 595 (2017).
3. S. Šesnić, S. Lalléchère, D. Poljak, A. Šušnjara, K.E.K. Drissi, *Electr. Power Syst. Res.* **190**, 106861 (2021).
4. L. Drewniak, S. Kochowski, *J. Mater. Sci. Mater. Electron.* **31** No 3, 19106 (2020).
5. G. Friesen, M.E. Özsar, E.D. Dunlop, *Thin Solid Films* **361-362**, 303 (2000).
6. S. Kochowski, K. Nitsch, *Thin Solid Films* **415** No 1-2, 133 (2002).
7. C. Guillaume, C. Labbé, C. Frilay, J.-L. Doualan, F. Lemarié, L. Khomenkova, L. Borkovska, X. Portier, *Phys. Status Solidi A* **216** No 2, 1800203 (2018).
8. X.C. Wang, X.M. Chen, B.H. Yang, *J. Alloy. Compd.* **488** No 1, 232 (2009).
9. *Handbook of Optical Constants of Solids* (Ed. by E.D. Palik) (San Diego: Academic: 1998).
10. R.C. Rai, M. Guminiak, S. Wilser, B. Cai, M.L. Nakarmi, *J. Appl. Phys.* **111** No 7, 073511 (2012).
11. A. Podolian, V. Kozachenko, A. Nadtochiy, N. Borovoy, O. Korotchenko, *J. Appl. Phys.* **107** No 9, 093706 (2010).
12. V. Schmid, V. Kuryliuk, A. Nadtochiy, O. Korotchenko, P.-W. Li, 39th International Conference on Electronics and Nanotechnology (*ELNANO-2019*), 92 (Kyiv: IEEE: 2019).
13. C. Munakata, K. Yagi, T. Warabisako, M. Nanba, S. Matsubara, *Jpn. J. Appl. Phys.* **23**, 1451 (1984).
14. O. Wing, *Classical Circuit Theory* (New York: Springer: 2008).
15. S.G. Johnson, *The NLOpt nonlinear-optimization package*, <http://github.com/stevengj/nlopt>.
16. K.S. Suresh Kumar, *Electric Circuit Analysis* (India: Pearson: 2013).
17. S. Havlin, D. Ben-Avraham, *Adv. Phys.* **51** No 1, 187 (2002).
18. B.O. Agudelo, W. Zamboni, É. Monmasson, *Energies* **14**, 4415 (2021).
19. J.A. López-Villanueva, S. Rodríguez-Bolívar, *Energies* **15**, 792 (2022).
20. B. Hussain, A. Aslam, T.M. Khan, M. Creighton, B. Zohuri, *Electronics* **8**, 238 (2019).

Моделювання за допомогою методу еквівалентних схем перехідних процесів при збудженні поверхневої фото-ЕРС в тонких плівках ZnO

А. Надточій¹, А. Подолян¹, О. Коротченков¹, О. Оберемок², О. Косуля², Б. Романюк²

¹ Фізичний факультет, Київський національний університет імені Тараса Шевченка, 01601 Київ, Україна
² Інститут Фізики напівпровідників ім. В. С. Лашкарєва НАН України, 03028 Київ, Україна

Плівки ZnO були отримані нанесенням оксиду цинку на підкладку кремнію р-типу за допомогою магнетронного розпилення, після чого у плівку були імплантовані іони Nd⁺ з подальшим відпалом. Динаміка фотозбуджених носіїв досліджувалась за допомогою вимірювання поверхневої фото-ЕРС. Перехідний процес кінетики фото-ЕРС після вимкнення джерела світла часто має вигляд немоного та/або знакозмінного загасання. Моделювання таких складних перехідних процесів проводилося за допомогою методу еквівалентних схем. Були розроблені еквівалентні схеми, що містять у собі декілька елементів опору (R), ємності (C) та індуктивності (L). За допомогою аналізу імпедансу в часовій області була також розроблена проста процедура підгонки, яка дозволяє точно відтворювати вимірний перехідний процес фото-ЕРС. Показано можливий взаємозв'язок між цими елементами RCL і фізичною картиною явищ переносу заряду в областях розділу структури. Такий підхід може бути корисним для використання при моделюванні характеристик інтерфейсів у напівпровідникових структурах і пристроях.

Ключові слова: Поверхнева фото-ЕРС, Оксид цинку, Еквівалентні схеми.